Eur. Phys. J. D **45**, 501–506 (2007)
DOI: 10.1140/epjd/e2007-00211-9

THE EUROPEAN PHYSICAL JOURNAL D

Cavity ring-down spectroscopy of metallic gold nanoparticles

S. Gilb[1,a], K. Hartl[1], A. Kartouzian[1], J. Peter[1], U. Heiz[1], H.-G. Boyen[2], and P. Ziemann[2]

[1] Lehrstuhl für Physikalische Chemie I, Technische Universität München, 85747 Garching, Germany
[2] Abteilung Festkörperphysik, Universität Ulm, 89069 Ulm, Germany

Received 27 April 2007
Published online 27 June 2007 –

Abstract. The optical properties of supported gold nanoparticles with sizes of 1.3 nm, 1.6 nm, 2.5 nm, and 2.9 nm have been studies by using cavity ring-down spectroscopy in the photon energy range between 1.8 eV and 3.0 eV. The obtained results show the possibility to obtain optical information of nanoassembled materials with high sensitivity. The experimental findings are compared to calculations using Mie-Drude theory. Whereas the broadening of the surface plasmon resonance with decreasing size is well described by this model, the observed blue-shift of the surface plasmon resonance contradicts the predictions of the Mie-Drude theory. The latter effect can be explained by the presence of a skin region with decreased polarizability typical for coinage metal particles. Furthermore, it is found that the supported gold nanoparticles are robust under ambient conditions, an important issue when using these materials for optical applications.

PACS. 61.46.Df Nanoparticles

1 Introduction

Progress in nanoscience made new materials, consisting of monodispersed nanoclusters or nanoparticles with narrow size distributions, available [1–3]. Such materials can for instance be synthesized by cluster deposition from preformed molecular beams [1], the deposition of molecular precursors [3] or by self-assembly on surfaces [2]. The interest in such nanostructured materials, comes in part from their fascinating optical properties, which can be tuned in a sophisticated way by varying size or the chemical composition of the nanoparticles [4–6]. The unique optical properties of metal nanoparticles have their origin in the surface plasmon, which strongly depends on size, shape and surrounding of the particle [7–11]. Experimental studies of optical properties of nanoparticles on surfaces is not trivial, as the surface density of the particles has to be low, in order to keep the particles well separated. These, together with the relatively low absorption cross sections of small metal particles, prevent the use of regular spectroscopic methods to obtain optical information of such nanoassembled materials.

Cavity ring-down spectroscopy (CRDS) has been proven to be very sensitive and it has been applied successfully in the gas phase for studying transitions of molecules with low absorption cross sections at low densities [12–14]. A few studies demonstrated the feasibility to use cavity ring-down spectroscopy (CRDS) for the optical characterization of thin films or particles supported on transparent samples with high sensitivity [15–18]. CRDS is based on an optical cavity built of two highly reflective mirrors ($R > 99.99$), in which a short light pulse of a given wavelength is introduced. By measuring the lifetime of the light pulse inside the cavity (called ring-down time), one is able to determine the intrinsic loss of the cavity due to transmission through the mirrors, scattering losses and in the present case losses from the support material inside the cavity. This intrinsic loss of the support material can be compared to the one obtained after nanoparticle preparation on the support material, resulting in the loss due to the nanoparticles. The losses of the nanoparticles as function of wavelength correspond to the absorption spectrum of the respective nanoparticles. In this work we apply CRDS for studying two dimensional arrays of gold nanoparticles with sizes ranging from ∼1 nm up to ∼3 nm on amorphous SiO_2 and discuss the experimental findings with the aid of classical Mie-Drude theory.

2 Experimental

2.1 Preparation of the particles

The preparation of the nanoparticles is described in detail elsewhere and will be only briefly discussed here [2,19] It is based on a two step process. First, spherical reverse micelles are formed by dissolving polystyrene (PS)-*block*-poly(2-vinylpyridine) in an apolar solvent such as toluene. A metal salt, in this case $HAuCl_4$ is added to the solution and the salt slowly migrates into the core of the micelles while carefully stirring the micelle solution. At equilibrium, all micelles are loaded with an equal

[a] e-mail: Stefan.Gilb@mytum.de

amount of metal salt, resulting in a small size dispersion of the final metal particles. The loaded micelles are transferred onto the substrate by dip coating. At this stage, the loaded micelles are distributed on the substrate in a hexagonal arrangement. Removing the ligand polymer and reducing the metal precursor salt to pure metal are done by exposing the "monomicellar" layer to an oxygen plasma. X-ray photoelectron spectroscopy experiments revealed that after the oxygen plasma treatment gold oxides are formed. After an annealing step, or alternatively after storing at ambient conditions for several days, the Au_2O_3 is completely reduced to Au [20]. It has been observed previously that the original order of the micellar arrangement is conserved, and a two dimensional array of hexagonally arranged nanoparticles is obtained [20]. Typical size distributions were measured by AFM to be e.g. 2.9 nm $\pm$ 0.5 nm, or 1.3 $\pm$ 0.3 nm [2]. It has also been shown that on sapphire and silicon supports the particles have a nearly spherical shape, and it is assumed that this is also true on the silica substrates used in this work [19].

For the CRDS experiments a transparent substrate is required to perform the measurements; for this reason microscopy coverslip plates with a thickness of 0.13–0.16 mm were used as substrate materials. The dip coating was done for half of the glass substrate, resulting in substrates, which are half covered on both sides with micelles. The investigated samples were the result of two different batches. The first batch includes the nanoparticles with an average diameter of 2.9 nm, 1.6 nm, and 1.3 nm, respectively and was stored for more than 9 months before the experiments were carried out. A second batch was used to produce samples with an average diameter of 2.9 nm and was measured about one month after preparation. The samples were stored under ambient conditions between preparation and measurement. The measurements also were done under ambient condition.

2.2 CRD setup

The optical setup is illustrated in Figure 1. A stable ring-down cavity is formed by 2 confocal mirrors (Los Gatos Research Inc.) with a focal length of 6 m and a cavity length of 1.38 m. The pulsed radiation is produced by a Nd:YAG-laser-pumped midband optical parametric oscillator (OPO) (Innolas SpitLight-1200, GWU VisIR2/400 ULD) with a bandwidth below 7 cm^{-1} and a pulse length of $\approx$7 ns. The output energy varies between $\approx$10 mJ and 20 mJ per pulse depending on the wavelength. No special mode matching optics are used to adapt the laser profile to the cavity modes, but pinholes along the laser path are used to simplify the day to day alignment and select a homogeneous part of the otherwise rather large, nearly rectangular laser beam of the OPO-laser. The light is linearly polarized by a Glan-laser-polarizer directly in front of the cavity. The laser pulse injected into the cavity remains in the cavity for several microseconds. Its intensity is reduced after every round trip by the losses at the mirrors (scattering, transmission), and absorption and scattering losses of the sample. The light leaking out of the second cavity

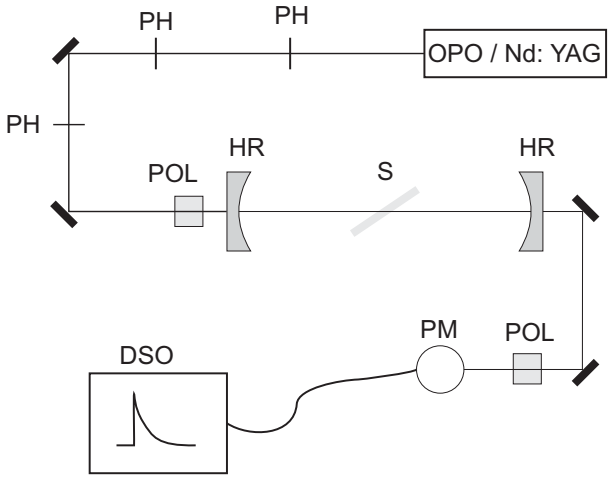

Fig. 1. Schematic illustration of the optical setup used in the experiment. PH: pinholes, HR: high reflective mirrors, POL: polarizers, PM: photomultiplier, DSO: digital oscilloscope, S: sample at Brewster's angle.

mirror is detected and amplified with a photomultiplier (Hamamatsu 7732-10). A rotatable polarizer in front of the photomultiplier serves as variable intensity attenuator and prevents saturation of the photomultiplier tube. The signal from the photomultiplier is fed into an 8 bit digital storage oscilloscope (LeCroy Waverunner 6051), which measures single traces and saves them to the internal hard drive.

The wavelength scans are fully automated. The wavelength dependent output power of the OPO as well as the strongly wavelength dependent reflectivity of the cavity mirrors, require a change of the photomultiplier sensitivity to use the full dynamic range of the photomultiplier and the oscilloscope. This is done automatically by a home written LabView program for every measured wavelength by means of a lookup table. The LabView program runs on the internal computer of the oscilloscope, and also controls the wavelength settings of the OPO-laser. The used cavity mirrors cover only 30 to 70 nm around a center wavelength. To cover the entire wavelength range from 420 nm to 700 nm, we use 6 cavities centered at wavelengths of 430 nm, 480 nm, 520 nm, 570 nm, 610 nm and 640 nm, respectively. The cavity mirrors are chosen to have a minimum of 6 nm spectral overlap between the different cavities. However, typically an overlap between the cavities of more than 15 nm is achieved.

To determine the ring-down time at each measured point, 80 single ring-down traces were acquired. To each trace a single exponential decay according to the function

$$I(t) = I_0 + I_1 \exp\left(-\frac{t}{\tau}\right) \quad (1)$$

is fitted using the nonlinear Levenberg-Marquardt method. I_0 and I_1 are the offset and a scaling factor, respectively; τ is the ring-down time. Due to instabilities of the laser system, about 1–4% of the laser shots have intensities close to zero, resulting in meaningless negative or

unrealistically large ring-down times in the order of ms. To prevent a corruption of the mean ring-down time by these single events, only ring-down times in a range of ±100% of the median ring-down time were averaged to obtain a final value for a given wavelength point. The outlier percentage was in no case above 4% (e.g. 3 out of 80 measurements). From the averaged ring-down time τ, the cavity length L, and the speed of light c, the loss can be calculated by:

$$\Lambda = 1 - \exp\left(-\frac{L}{c}\frac{1}{\tau}\right). \tag{2}$$

While the shot to shot standard deviation is in the order of 5%, the overall noise can be estimated directly from the scatter between adjacent data points in the obtained spectra and is typically ≈±140 ppm (see e.g. Fig. 3).

The main challenge in using solid samples in CRDS is the intrinsic loss due to scattering from the sample surfaces. One way to minimize these losses is to mount the glass slide perfectly perpendicular to the cavity axis, keeping reflection losses from the surfaces inside the cavity. The disadvantage of this method is the elaborate alignment that is required, since the slightest misalignment increases the loss by orders of magnitudes. The second method is the alignment of the sample at Brewster's angle, in which no reflections from the optical surfaces are to be expected. Due to the insensitivity of the reflectivity as a function of the angle around Brewster's angle (≈56°), the alignment is rather insensitive. Also, by putting the sample at Brewster's angle, the polarization of the light inside the cavity is fixed to p-polarization with respect to the sample. With the coverslip plates used in the preparation of the nanoparticles, the first method, with a perpendicular alignment of the sample was not only difficult to achieve, but also inferior in terms of losses compared to Brewster's angle configuration, which is rather easy to obtain. We attribute this to the imperfect planarity of the coverslip plates. In all measurements present here, the Brewster's angle configuration was used. The Brewster's angle of the sample was aligned prior to measurement for every one of the six cavities at the center wavelength of the corresponding cavity. We note that even in the case of the substrate to be well-aligned at Brewster's angle, losses of 1000–2000 ppm were observed, which is an order of magnitude higher than what is to be expected from absorption of a thin glass plate. This is partly due to the fact, that cleaning of the samples after preparation of the nanoparticles is not possible. But also in the case of freshly cleaned coverslip plates, we find high losses, which we attribute to the birefringence of the plates effectively creating small contributions of s-polarization at every pass through the sample. This polarization component is, due to reflection at the sample surface, not stable in the cavity.

3 Theory

The Mie-Drude theory is used to describe the spectra of nanoparticles in the size range considered here. The theory describes scattering and absorption of a plane wave by a single sphere [21]. The derivation of the theory and application to nanoparticles can be found, for example, in reference [22]. We followed the method of implementation described in references [23,24] and only a brief description will be given here. The particle and the surrounding media are considered as homogeneous and are described by the bulk optical dielectric functions. Since the size of the particles is much smaller than the wavelength of the exciting radiation, the discussion can be restricted to the dipole term in the multipole expansion of the solution of the Maxwell equations. The cross section in the dipole approximation is then given by:

$$\sigma = 9\varepsilon_m^{3/2} V_0 \frac{\omega}{c} \frac{\varepsilon_2(\omega)}{\left[\varepsilon_1(\omega) + 2\varepsilon_m\right]^2 + \varepsilon_2^2(\omega)} \tag{3}$$

with ω and c being the frequency and the speed of light, respectively, ε_m the dielectric constant of the media surrounding the nanoparticle, and V_0 being the volume of the particle. $\varepsilon_1(\omega)$ and $\varepsilon_2(\omega)$ are the real and imaginary part of the dielectric constant of the absorbing solid. In the Mie-Drude model, the size effect is introduced by a size dependent scattering rate which alters the free electron contribution to the dielectric function. The scattering rate of the bulk, Γ_∞ is increased through a size dependent scattering rate. The latter can be interpreted as the average rate, with which the excited plasmon hits the outside of the particle. The total scattering rate ω_s is thus equal to:

$$\omega_s = \Gamma_\infty + A\frac{v_F}{R}. \tag{4}$$

In this equation R is the radius of the particle and v_F is the Fermi velocity ($v_F = 1.4 \times 10^8$ cm/s for gold) [25]. The proportional factor, A, is a model dependent parameter and his value depends on the type of scattering assumed. This parameter, essential a size scaling parameter, takes the value of unity for isotropic scattering or 3/4 if diffusive scattering is assumed. The value of 1, which corresponds to an isotropic scattering, is used throughout the calculations in this work. To incorporate the scattering into the dielectric function, the latter is separated into the free-electron (Drude) contribution ($\varepsilon_{1\mathrm{D}/2\mathrm{D}}(\omega)$) from the s-electrons and the interband contribution ($\varepsilon_{\mathrm{I1B}/2\mathrm{IB}}(\omega)$) originating from the d-electrons

$$\varepsilon_1(\omega) = \varepsilon_{1\mathrm{IB}}(\omega) + \varepsilon_{1\mathrm{D}}(\omega)\,, \quad \varepsilon_2(\omega) = \varepsilon_{2\mathrm{IB}}(\omega) + \varepsilon_{2\mathrm{D}}(\omega). \tag{5}$$

The free electron part for the bulk can be calculated by:

$$\varepsilon_{1\mathrm{D}}(\omega) = 1 - \frac{\omega_\mathrm{P}^2}{\omega^2 + \Gamma_o^2}\,, \quad \varepsilon_{2\mathrm{D}}(\omega) = \frac{\omega_\mathrm{P}^2 \Gamma_o}{\omega\left(\omega^2 + \Gamma_o^2\right)}. \tag{6}$$

Here ω_P is the plasma frequency corresponding to 8.89 eV for gold, Γ_∞ is the plasmon scattering rate in the bulk gold and corresponds to 1.11×10^{14} s^{-1} for gold. The dielectric function from bulk can be found in [26]. From there $\varepsilon_{1\mathrm{D}/2\mathrm{D}}(\omega)$ can be determined. In Figure 2 the size evolution of the spectrum predicted by this model is shown. For the case of a 2 nm particles it is shown how a size dispersion of ±0.5 nm affects the spectral response of the nanoparticle in the framework of the Mie-Drude theory.

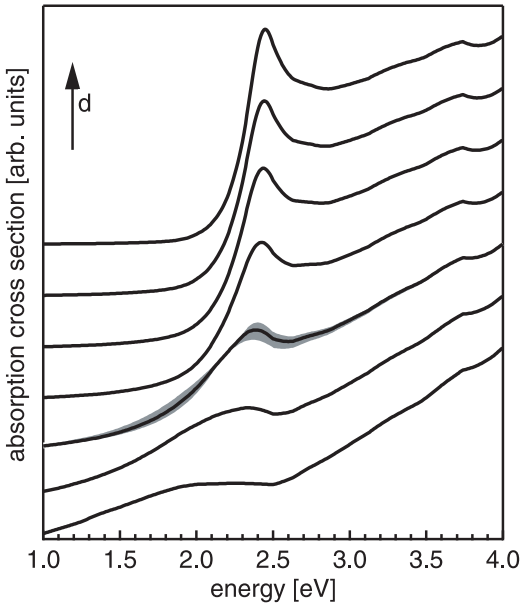

Fig. 2. Absorption cross sections calculated by the Mie-Drude theory as explained in the text. The spectra were normalized to an equal absorption at 4 eV and vertically shifted. The diameters used in the simulation are: 0.5, 1, 2, 5, 10, 20 nm and bulk.

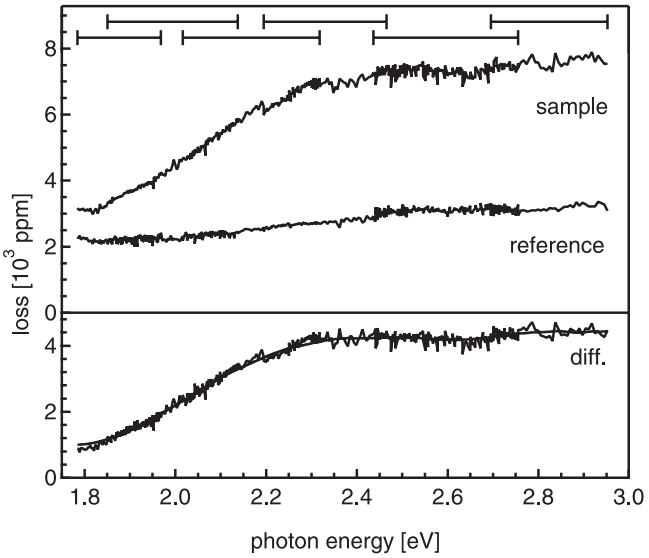

Fig. 3. Illustration of the reference method employed to disentangle the contribution from the support. Shown is the measured spectrum of the area with nanoparticles (sample) and the area without nanoparticles (reference). The difference of these two spectra is regarded as the absorption of the nanoparticles. Note, that the traces are not shifted and represent the real losses. The gold nanoparticles used in these studies have an average diameter of 2.5 nm. The solid line the difference spectrum represents moving averaged data to guide the eye. On the top of the graph the spectral ranges of the used cavities are illustrated by horizontal lines.

4 Results and discussion

To acquire the whole spectrum from 1.78 eV to 2.95 photon energy we used 6 different cavity mirror sets, centered at different wavelengths. We denoted the range of the used cavities in Figure 3. Each individual run obtained by using a single cavity was scaled by a factor, S, to achieve reasonable overlap of the measured losses between adjacent cavities. The values of S were between 0.85 and 1.15. This uncertainty is caused by day to day variation of the measured losses and it is attributed to changes of the area on the sample probed by the laser beam. In fact, we found that the measured loss shows a dependence on the substrate position. Since this is true also for the *reference*, e.g. the uncoated part of the substrate (see below), we attribute this effect to the oxygen plasma treatment. It may lead to a random modification of the substrate surface. Thus, the alignment of the laser beam and laser mode fluctuations are very important.

To obtain the absorption spectra of the nanoparticles, the contribution to the absorption from the SiO_2 support has to be subtracted. To obtain a reference spectrum the following procedure was carried out. The samples were prepared in such a way that only half of the area was dip coated with nanoparticles. Thus, the region with the nanoparticles was used for *sample* measurement, whereas the uncoated area served as *reference*. To minimize errors due to inhomogeneities of the substrate, a *sample* and a *reference* point was picked prior to the measurement and kept identical throughout the measurement. Figure 3 shows measurements of the sample and reference spectra taken at an area with gold nanoparticles with mean diameters of 2.5 and an area of the clean SiO_2 support, respectively. The difference spectrum is also shown in Figure 3 and it is attributed to the pure absorption spectrum of the respective nanoparticles. Despite the alignment of the substrate at Brewster's angle, the uncoated substrate shows a considerable extinction of light due to birefringence, absorption and scattering as mentioned above. More important, however, the reference spectrum is structureless and the loss increases linearly with the photon energy as shown in Figure 3. This characteristic behavior is typical for all SiO_2 support materials used so far, whether they were treated by sputter-oxidation during sample preparation or whether they were new and untreated. Note, that for the lowest photon energy the loss in the difference spectrum shown in Figure 3 is not close to zero as one would expect for gold nanoparticles in the size range above 2 nm [22]. This indicates that in the present measurements there is an offset, which varies from sample to sample (cf. also Fig. 4). As described above and in contrast to the invariant spectral response of the substrate, the absolute losses measured at different positions of the substrate is inhomogeneous. This, however, results in an absolute shift of the loss in the difference spectra. It is important to note that the distinct spectral structure observed in the difference spectra can, however, unambiguously be attributed to the optical response of the nanoparticles alone and does not originate from spectral fluctuations in the reference measurements of the substrate. In Figures 3 and 4 no baseline correction was carried out in order to correct for this offset. The theoretical

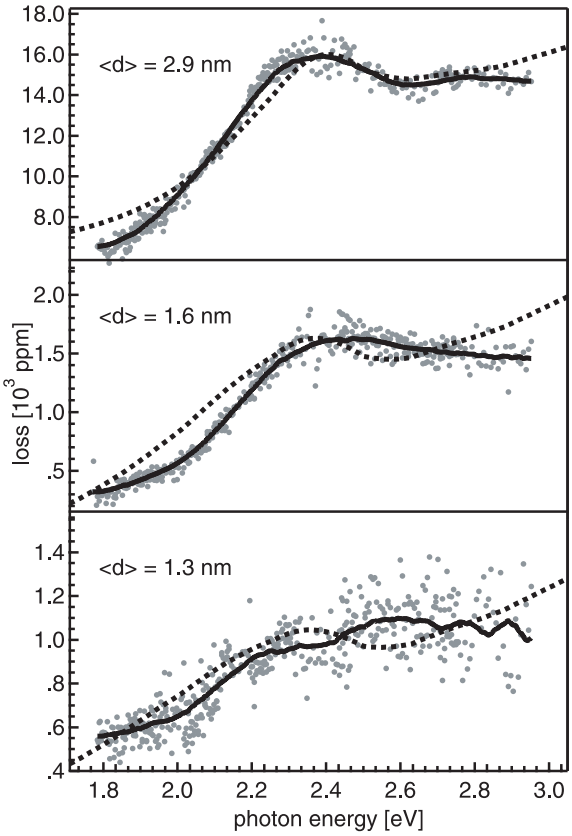

Fig. 4. Experimental data for supported nanoparticles of different mean diameters, $\langle d \rangle$ ($\langle d \rangle = 1.3$ nm, 1.6 nm, 2.9 nm). The solid line is a moving average to guide the eye. The y-scaling is proportional to d [3] and chosen to reflect the volume dependence of the absorption cross section. We assume that the loss of the nanoparticles is close to zero at the lowest photon energy and set the offset of the y-axis for the theoretical spectra accordingly (see text). The theoretical spectra are obtained by using the Mie-Drude theory and are represented as dotted lines.

spectra shown in Figure 4, however, were shifted in order to account for the offset with respect to the measured loss found at 1.8 eV.

Figure 4 depicts the spectra of the nanoparticles obtained after subtraction of the reference spectrum. Whereas the average sizes of the nanoparticles were changed from 1.3 nm, 1.6 nm, and 2.9 nm, the average nearest neighbor distance was similar for all samples ($\approx$35 nm), resulting in similar nanoparticle densities on the surface. The scaling factors of the three y-coordinates were chosen to be proportional to the volumes of the corresponding nanoparticles, in order to correct for the proportionality of the absorption cross section to the volume of the three nanoparticles as predicted by the Mie-Drude model (cf. Eq. (3)). Indeed, a first look at the spectra is in agreement with the prediction that the absolute absorption cross section scales with the particle's volume. Furthermore all spectra show an onset in the absorption above 1.8 eV. Maximal absorption cross sections are observed for energies around 2.4 eV, which corresponds to the energy of the surface plasmon resonance (SPR) peak. For the nanoparticles studied here, the surface plasmon peak is not as distinct as it is for matrix isolated silver nanoparticles or larger gold nanoparticles [22,27]. This behavior is well predicted by the Mie-Drude theory as displayed in Figures 3 and 4 [28]. The physical reason is the considerable lowering of the lifetime due to scattering at the particle boundaries, an effect which is enhanced for small particles. Smaller lifetimes result in a broadening of the SPR. As the onset of the interband transition in gold is below 2 eV these two contributions to the oscillator strength merge. Also this effect is well described by the Mie-Drude theory as shown by the simulated spectra in Figure 4 (dashed line). Similar effects have been observed for gold nanoparticles smaller than about 4 nm stabilized in various matrices like alumina or glass [6,22,24] and in solution [23].

While in the case of free alkali clusters a red shift of the SPR with decreasing cluster size has been measured [29], our data show a slight blue shift of the energy of maximal absorption when decreasing the mean particle diameter from 2.9 nm to 1.6 nm. This blue shift is in contradiction with the Mie-Drude theory, as it predicts a slight red-shift as shown in Figure 2. This observed blue shift, however, is in agreement with other experimental findings for coinage metal nanoparticles in the same size range [24]. For the coinage metals, the higher localization of the d-electrons compared to the s-electrons leads to an ineffective ion polarizability in the outer rim of the nanoparticles [24,30]. This concept, introduced by Liebsch [31], predicts an alteration of the dielectric function. Lermé et. al integrated this alteration into semi-quantal theoretical calculation, and was able to explain the observed blue shift. The standard Mie-Drude model is indeed not able to describe this effect, since the bulk dielectric function is used throughout the nanoparticle. An extension of the Mie-Drude theory to take this surface effect into account is possible, but is beyond the scope of this experimental publication [32].

Further, we see no influence of the substrate, while in a former study on gold atoms and dimers a strong influence of surface defects has been observed [16,33]. In that study we showed that the observed optical transitions involves electronic states, which are localized in the substrate-gold bond. This one electron transitions are orders of magnitude smaller than the collective electron excitations observed here.

5 Conclusion

In this work we measured for the first time the size evolution of two-dimensional hexagonally ordered arrays of gold nanoparticles in a size range of 1.3 nm up to 2.9 nm by using CRDS. This possibility clearly reveals the high sensitivity of CRDS in comparison with other optical methods. The measured spectra show typical characteristics of small gold particles, which proves the long term stability of these two dimensional nanostructures against complete oxidation even under ambient conditions. The experimental findings were discussed within the Mie-Drude theory

and we found a good description of the broadening of the SPR with decreasing size. The red-shift predicted by the Mie-Drude theory is not found in our experiments. This finding is in accordance with other experimental results on coinage metal nanoparticles, and can be explained by the presence of a skin region with decreased polarizability.

This research is supported by the Deutsche Forschungsgemeinschaft within the priority program SPP1153. We also acknowledge support from the European Project GSOMEN (contract No. 1549).

References

1. S. Gilb, M. Arenz, U. Heiz, Mat. Today **9**, 49 (2006)
2. H.G. Boyen, G. Kastle, F. Weigl, B. Koslowski, C. Dietrich, P. Ziemann, J.P. Spatz, S. Riethmuller, C. Hartmann, M. Möller, G. Schmid, M.G. Garnier, P. Oelhafen, Science **297**, 1533 (2002)
3. T.M. Bernhardt, B. Kaiser, K. Rademann, Phys. Chem. Chem. Phys. **4**, 1192 (2002)
4. M. Bruchez, M. Moronne, P. Gin, S. Weiss, A.P. Alivisatos, Science **281**, 2013 (1998)
5. Y.G. Sun, Y.N. Xia, Analyst **128**, 686 (2003)
6. B. Palpant, B. Prevel, J. Lerme, E. Cottancin, M. Pellarin, M. Treilleux, A. Perez, J.L. Vialle, M. Broyer, Phys. Rev. B **57** 1963 (1998)
7. C.L. Haynes, R.P.V. Duyne, J. Phys. Chem. B **105**, 5599 (2001)
8. Y.Y. Yu, S.S. Chang, C.L. Lee, C.R.C. Wang, J. Phys. Chem. B **101**, 6661 (1997)
9. D. Sarkar, N.J. Halas, Phys. Rev. E **56**, 1102 (1997)
10. S. Underwood, P. Mulvaney, Langmuir **10**, 3427 (1994)
11. U. Kreibig, L. Genzel, Surf. Sci. **156**, 678 (1985)
12. G. Berden, R. Peeters, G. Meijer, Inter. Rev. Phys. Chem. **19**, 565 (2000)
13. M.D. Wheeler, S.M. Newman, A.J. Orr-Ewing, M.N.R. Ashfold, J. Chem. Soc. Faraday Trans. **94**, 337 (1998)
14. J.J. Scherer, J.B. Paul, A. Okeefe, R.J. Saykally, Chem. Rev. **97**, 25 (1997)
15. A.C.R. Pipino, J.T. Woodward, C.W. Meuse, V. Silin, J. Chem. Phys. **120**, 1585 (2004)
16. J.M. Antonietti, M. Michalski, U. Heiz, H. Jones, K.H. Lim, N. Rösch, A.D. Vitto, G. Pacchioni, Phys. Rev. Lett. **94**, (2005)
17. R. Engeln, G.V. Helden, A.J.A.V. Roij, G. Meijer, J. Chem. Phys. **110**, 2732 (1999)
18. R.N. Muir, A.J. Alexander, Phys. Chem. Chem. Phys. **5**, 1279 (2003)
19. H.G. Boyen, G. Kastle, K. Zurn, T. Herzog, F. Weigl, P. Ziemann, O. Mayer, C. Jerome, M. Möller, J.P. Spatz, M.G. Garnier, P. Oelhafen, Adv. Funct. Mat. **13**, 359 (2003)
20. G. Kastle, H.G. Boyen, F. Weigl, G. Lengl, T. Herzog, P. Ziemann, S. Riethmuller, O. Mayer, C. Hartmann, J.P. Spatz, M. Möller, M. Ozawa, F. Banhart, M.G. Garnier, P. Oelhafen, Adv. Funct. Mat. **13**, 853 (2003)
21. G. Mie, Ann. Physik **25**, 377 (1908)
22. U. Kreibig, M. Vollmer, *Optical Properties of Metal Clusters* (Springer, Berlin, 1995)
23. M.M. Alvarez, J.T. Khoury, T.G. Schaaff, M.N. Shafigullin, I. Vezmar, R.L. Whetten, J. Phys. Chem. B **101**, 3706 (1997)
24. E. Cottancin, G. Celep, J. Lerme, M. Pellarin, J.R. Huntzinger, J.L. Vialle, M. Broyer, Theor. Chem. Acc. **116**, 514 (2006)
25. U. Kreibig, C. Vonfrags, Z. Phys. **224**, 307 (1969)
26. P.B. Johnson, R.W. Christy, Phys. Rev. B **6**, 4370 (1972)
27. E. Cottancin, J. Lerme, M. Gaudry, M. Pellarin, J.L. Vialle, M. Broyer, B. Prevel, M. Treilleux, P. Melinon, Phys. Rev. B **62**, 5179 (2000)
28. H. Hovel, S. Fritz, A. Hilger, U. Kreibig, M. Vollmer, Phys. Rev. B **48**, 18178 (1993)
29. C. Brechignac, P. Cahuzac, N. Kebaili, J. Leygnier, A. Sarfati, Phys. Rev. Lett. **68**, 3916 (1992)
30. J. Lerme, B. Palpant, B. Prevel, E. Cottancin, M. Pellarin, M. Treilleux, J.L. Vialle, A. Perez, M. Broyer, Eur. Phys. J. D **4**, 95 (1998)
31. A. Liebsch, Phys. Rev. B **48**, 11317 (1993)
32. S. Fedrigo, W. Harbich, J. Buttet, Phys. Rev. B **47**, 10706 1993
33. A.D. Vitto, G. Pacchioni, K.H. Lim, N. Rösch, J.M. Antonietti, M. Michalski, U. Heiz, H. Jones, J. Phys. Chem. B **109**, 19876 (2005)